

Differential Cross Sections for Neutron-Proton Scattering in the Region of the $d^*(2380)$ Dibaryon Resonance

P. Adlarson,¹ W. Augustyniak,² W. Bardan,³ M. Bashkanov,⁴ F.S. Bergmann,⁵ M. Berłowski,⁶ H. Bhatt,⁷ M. Büscher,^{8,9} H. Calén,¹ I. Ciepał,³ H. Clement,^{10,11} D. Coderre,^{12,13,*} E. Czerwiński,³ K. Demmich,⁵ E. Doroshkevich,^{10,11} R. Engels,¹² A. Erven,¹⁴ W. Erven,¹⁴ W. Eyrych,¹⁵ P. Fedorets,^{12,16} K. Föhl,¹⁷ K. Fransson,¹ F. Goldenbaum,¹² P. Goslawski,⁵ A. Goswami,^{12,18} K. Grigoryev,^{19,20} C.-O. Gullström,¹ F. Hauenstein,¹⁵ L. Heijkinskjöld,¹ V. Hejny,¹² M. Hodana,³ B. Höistad,¹ N. Hüskens,⁵ A. Jany,³ B.R. Jany,³ T. Johansson,¹ B. Kamys,³ G. Kemmerling,¹⁴ F.A. Khan,¹² A. Khoukaz,⁵ D.A. Kirillov,²¹ S. Kistryn,³ H. Kleines,¹⁴ B. Kłos,²² M. Krapp,¹⁵ W. Krzemień,²³ P. Kulesa,²⁴ A. Kupść,^{1,6} K. Lalwani,^{7,†} D. Lersch,¹² B. Lorentz,¹² A. Magiera,³ R. Maier,¹² P. Marciniowski,¹ B. Mariański,² M. Mikirtychiants,^{12,13,20} H.-P. Morsch,² P. Moskal,³ H. Ohm,¹² I. Ozerianska,³ E. Perez del Rio,^{10,11,‡} N.M. Piskunov,²¹ P. Podkopał,³ D. Prasuhn,¹² A. Pricking,^{10,11} D. Pszczel,^{1,6} K. Pysz,²⁴ A. Pysznik,^{1,3} C.F. Redmer,^{1,§} J. Ritman,^{12,13} A. Roy,¹⁸ Z. Rudy,³ S. Sawant,^{7,12} S. Schadmand,¹² T. Sefzick,¹² V. Serdyuk,^{12,25} R. Siudak,²⁴ T. Skorodko,^{10,11,26} M. Skurzok,³ J. Smyrski,³ V. Sopov,¹⁶ R. Stassen,¹² J. Stepaniak,⁶ E. Stephan,²² G. Sterzenbach,¹² H. Stockhorst,¹² H. Ströher,¹² A. Szczurek,²⁴ A. Täschner,⁵ A. Trzciniński,² R. Varma,⁷ M. Wolke,¹ A. Wrońska,³ P. Wüstner,¹⁴ P. Wurm,¹² A. Yamamoto,²⁷ L. Yurev,^{25,¶} J. Zabierowski,²⁸ M.J. Zieliński,³ A. Zink,¹⁵ J. Złomańczuk,¹ P. Żuprański,² and M. Żurek¹²
(WASA-at-COSY Collaboration)

R. L. Workman,²⁹ W. J. Briscoe,²⁹ and I. I. Strakovsky²⁹
(SAID Data Analysis Center)

A. Švarc^{30,31}

¹Division of Nuclear Physics, Department of Physics and Astronomy, Uppsala University, Box 516, 75120 Uppsala, Sweden

²Department of Nuclear Physics, National Centre for Nuclear Research, ul. Hoza 69, 00-681, Warsaw, Poland

³Institute of Physics, Jagiellonian University, ul. Reymonta 4, 30-059 Kraków, Poland

⁴Department of Physics, University of York, Heslington, York, YO10 5DD, UK

⁵Institut für Kernphysik, Westfälische Wilhelms-Universität Münster, Wilhelm-Klemm-Str. 9, 48149 Münster, Germany

⁶High Energy Physics Department, National Centre for Nuclear Research, ul. Hoza 69, 00-681, Warsaw, Poland

⁷Department of Physics, Indian Institute of Technology Bombay, Powai, Mumbai-400076, Maharashtra, India

⁸Peter Grünberg Institut, Forschungszentrum Jülich, 52425 Jülich, Germany

⁹Institut für Laser- und Plasmaphysik, Heinrich-Heine Universität Düsseldorf, 40225 Düsseldorf, Germany

¹⁰Physikalisches Institut, Eberhard-Karls-Universität Tübingen, Auf der Morgenstelle 14, 72076 Tübingen, Germany

¹¹Kepler Center for Astro and Particle Physics, University of Tübingen, Auf der Morgenstelle 14, 72076 Tübingen, Germany

¹²Institut für Kernphysik, Forschungszentrum Jülich, 52425 Jülich, Germany

¹³Institut für Experimentalphysik I, Ruhr-Universität Bochum, Universitätsstr. 150, 44780 Bochum, Germany

¹⁴Zentralinstitut für Engineering, Elektronik und Analytik, Forschungszentrum Jülich, 52425 Jülich, Germany

¹⁵Physikalisches Institut, Friedrich-Alexander-Universität

Erlangen-Nürnberg, Erwin-Rommel-Str. 1, 91058 Erlangen, Germany

¹⁶Institute for Theoretical and Experimental Physics, State Scientific Center of the Russian Federation, Bolshaya Cheremushkinskaya 25, 117218 Moscow, Russia

¹⁷II. Physikalisches Institut, Justus-Liebig-Universität Gießen, Heinrich-Buff-Ring 16, 35392 Giessen, Germany

¹⁸Department of Physics, Indian Institute of Technology Indore, Khandwa Road, Indore-452017, Madhya Pradesh, India

¹⁹III. Physikalisches Institut B, Physikzentrum, RWTH Aachen, 52056 Aachen, Germany

²⁰High Energy Physics Division, Petersburg Nuclear Physics Institute,

Orlova Rosh 2, Gatchina, Leningrad district 188300, Russia

²¹Veksler and Baldin Laboratory of High Energy Physics, Joint

Institute for Nuclear Physics, Joliot-Curie 6, 141980 Dubna, Russia

²²August Chetkowski Institute of Physics, University of Silesia, Uniwersytecka 4, 40-007, Katowice, Poland

²³High Energy Physics Division, National Centre for Nuclear Research, 05-400 Otwock-wierk, Poland

²⁴The Henryk Niewodniczański Institute of Nuclear Physics, Polish

Academy of Sciences, 152 Radzikowskiego St, 31-342 Kraków, Poland

²⁵Dzhelepov Laboratory of Nuclear Problems, Joint Institute for Nuclear Physics, Joliot-Curie 6, 141980 Dubna, Russia

²⁶Department of Physics, Tomsk State University, 36 Lenin Ave., Tomsk, 634050 Russia

²⁷High Energy Accelerator Research Organisation KEK, Tsukuba, Ibaraki 305-0801, Japan

²⁸Astrophysics Division, National Centre for Nuclear Research, Box 447, 90-950 Łódź, Poland

²⁹*Data Analysis Center at the Institute for Nuclear Studies, Department of Physics, The George Washington University, Washington, D.C. 20052, U.S.A.*
³⁰*Rudjer Bošković Institute, Bijenička cesta 54, P.O. Box 180, 10002 Zagreb, Croatia*
³¹*Tesla Biotech, Mandlova 7, 10002 Zagreb, Croatia*
(Dated: October 25, 2021)

Differential cross sections have been extracted from exclusive and kinematically complete high-statistics measurements of quasifree polarized $\bar{n}p$ scattering performed in the energy region of the $d^*(2380)$ dibaryon resonance covering the range of beam energies $T_n = 0.98 - 1.29$ GeV ($\sqrt{s} = 2.32 - 2.44$ GeV). The experiment was carried out with the WASA-at-COSY setup having a polarized deuteron beam impinging on the hydrogen pellet target and utilizing the quasifree process $dp \rightarrow np + p_{\text{spectator}}$. That way the np differential cross section $\sigma(\Theta)$ was measured over a large angular range. The obtained angular distributions complement the corresponding analyzing power $A_y(\Theta)$ measurements published previously. A SAID partial-wave analysis incorporating the new data strengthens the finding of a resonance pole in the coupled ${}^3D_3 - {}^3G_3$ waves.

PACS numbers: 13.75.Cs, 13.85.Dz, 14.20.Pt
Keywords:

INTRODUCTION

Recently a resonance pole with $I(J^P) = 0(3^+)$ at $(2380 \pm 10 - i40 \pm 5)$ MeV — denoted $d^*(2380)$ — was discovered in the coupled ${}^3D_3 - {}^3G_3$ partial waves of nucleon-nucleon (NN) scattering by the SAID partial-wave analysis based on the full SAID data base and recent analyzing power data provided by WASA-at-COSY for the lab energy range $T_n = 1.095 - 1.270$ GeV ($\sqrt{s} = 2.36 - 2.43$ GeV) [1, 2]. The values for this pole coincide with a pronounced narrow resonance structure previously observed in the total cross section of the basic isoscalar double-pionic fusion reaction $pn \rightarrow d\pi^0\pi^0$ [3, 4] at a mass $M \approx 2370$ MeV with a width of $\Gamma \approx 70$ MeV. From the angular distributions spin-parity $J^P = 3^+$ was deduced [4]. Additional evidence for $d^*(2380)$ has been found recently in the $pn \rightarrow d\pi^+\pi^-$ [5], $pn \rightarrow pp\pi^0\pi^-$ [6], $pn \rightarrow pn\pi^0\pi^0$ [7] and $pn \rightarrow pn\pi^+\pi^-$ [8, 9] reactions. In measurements of the isoscalar single-pion production cross section no significant decay of this resonance into the isoscalar $[NN\pi]_{I=0}$ channel has been observed — providing a small upper limit [10]. That way all branchings of this resonance into the hadronic decay channels NN , $NN\pi$ and $NN\pi\pi$ have been extracted [10, 11]. They agree with the decay of a deeply bound $\Delta\Delta$ system [11, 12], possibly accompanied with a small admixture of a $D_{12}\pi$ configuration [13], where D_{12} denotes the $I(J^P) = 1(2^+)$ resonance structure near the ΔN threshold. For a discussion of the latter see, *e.g.*, Ref. [12]. Recently also suggestive evidence for a photo-excitation of $d^*(2380)$ has been found in measurements of the $\gamma d \rightarrow d\pi^0\pi^0$ reaction [14, 15].

In addition to the many evidences for the dibaryon resonance $d^*(2380)$ the establishment of its resonance pole in np scattering certainly is of particular importance. This finding is solely based on the analyzing power data provided by WASA-at-COSY. Hence it appears highly desirable to supplement this data base in the region of the $d^*(2380)$ resonance by comprehensive differential

cross section data, since previous measurements mainly covered just either the very forward [16] or the backward angle [17] region.

EXPERIMENT

For the extraction of the differential cross sections in the region of the $d^*(2380)$ resonance we use the same data set as exploited before for the extraction of the analyzing powers [1, 2]. For this purpose the np elastic scattering was measured in the quasifree mode with the WASA detector including a hydrogen pellet target [19, 20] at COSY (Forschungszentrum Jülich, Germany) and by using a polarized deuteron beam with an energy of $T_d = 2.27$ GeV. That way the full energy range of the conjectured resonance was covered. Note that we observe here the quasi-free scattering process $dp \rightarrow np + p_{\text{spectator}}$ in inverse kinematics, which allows to detect also the fast spectator proton in the forward detector of WASA.

Since we deal here with events originating from channels with large cross section, the trigger was set to at least one hit in the first layer of the forward range hodoscope. For the case of quasifree np scattering this defines two event classes with each of them having the spectator proton detected in the forward detector:

- scattered proton and scattered neutron both detected in the central detector covering the neutron angle region $40^\circ < \Theta_n^{cm} < 125^\circ$
- scattered proton detected in the forward detector with the scattered neutron being unmeasured covering thus $132^\circ < \Theta_n^{cm} < 145^\circ$

That way a large range of neutron scattering angles could be covered.

For each selected event one neutral hit in the central detector was required. The pn elastic events have been identified by using the kinematic constraints for opening angle and planarity.

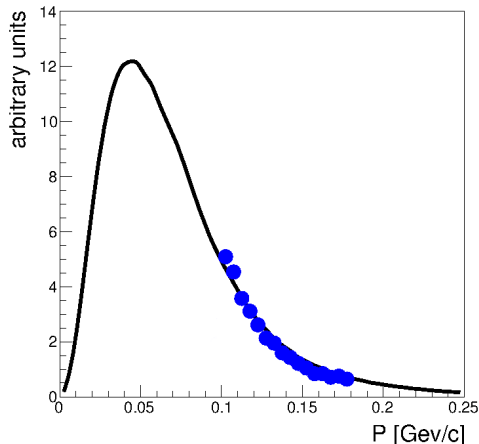


FIG. 1: Distribution of the spectator proton momenta P (in the deuteron rest frame) in the $dp \rightarrow pn + p_{\text{spectator}}$ reaction. Data are given by the full circles. The solid line shows the expected distribution for the quasifree process based on the CD Bonn potential [21] deuteron wavefunction. For the data analysis only events with spectator momenta $P < 0.18$ GeV/c have been used.

Since by use of the inverse kinematics the spectator proton is in the beam particle, the deuteron, the spectator is very fast. This allows its detection in the forward detector and by reconstruction of its kinetic energy and its direction the full four-momentum of the spectator proton has been determined.

Similarly the four-momentum of the actively scattered proton has been obtained from its track information in either forward or central detector (in the latter case the energy information was not retrieved).

Since the neutron has been detected by a hit in the calorimeter (composed of 1012 CsI(Na) crystals) of the central detector— associated with no hit in the preceding plastic scintillator barrel —, only its directional information has been obtained. In the subsequent kinematical fit the full event could be reconstructed with two overconstraints in case of the first event class and with three overconstraints in case of the second event class.

As noted above, we utilize here data, which have been obtained by use of a polarized beam for the determination of analyzing powers. Hence, in order not to distort the beam polarization, the magnetic field of the solenoid in the central detector was switched off in that beamtime.

Whereas in analyzing power measurements detector efficiencies cancel out, the determination of differential cross sections heavily depends on a precise knowledge of detector efficiencies. The latter have been determined by comprehensive Monte-Carlo (MC) simulations of the WASA detector performance and their cross check against calibration data.

The momentum distribution of the observed specta-

tor proton in the elastic np scattering process is plotted in Fig. 1 in the deuteron rest frame and compared with Monte Carlo simulations of the proton momentum distribution in the deuteron. In these simulations the deuteron wavefunction of CD Bonn potential [21] has been used. Because of the beam-pipe ejectiles can only be detected in the forward detector for lab angles larger than 2.5 degrees. In order to assure a quasi-free process we omit events with spectator momenta larger than 0.18 GeV/c (in the deuteron rest system) from the subsequent analysis — similar to what was done in previous work [4–6].

The absolute normalization of our data has been obtained by normalizing our data at $T_p = 1.109$ GeV to the backangle data of Bizard *et al.* [17].

For a cross check of the absolute normalization of the np scattering data we have analyzed the $dp \rightarrow np\pi^0 + p_{\text{spectator}}$ reaction, which has been taken in parallel and with the same trigger. Since there are no high-quality data for the $np\pi^0$ channel at the energy of interest here, we have used the following isospin relation for the total cross sections [18]

$$2\sigma(np \rightarrow np\pi^0) = \sigma(pp \rightarrow pn\pi^+) + 2\sigma(np \rightarrow pp\pi^-) - 2\sigma(pp \rightarrow pp\pi^0) \quad (1)$$

Using the values 17 ± 2.2 mb [8], 2.5 ± 0.2 mb and 4.0 ± 0.3 mb [10] for the total cross sections of the $pp \rightarrow pn\pi^+$, $np \rightarrow pp\pi^-$ and $pp \rightarrow pp\pi^0$ reactions, respectively, we arrive at a total cross section 6 ± 1 mb for the $np \rightarrow np\pi^0$ reaction. Using the absolute normalization as obtained from the adjustment of our np data to those of Bizard *et al.*, we arrive at 7 mb for the $np \rightarrow np\pi^0$ reaction — in good agreement with the value obtained from the isospin relation.

EXPERIMENTAL RESULTS

Due to the Fermi motion of the nucleons bound in the beam deuteron, the measurement of the quasi-free np scattering process covers a range of energies in the np system. Meaningful statistics could be collected for the range of np center-of-mass energies $2.32 < \sqrt{s} < 2.44$ corresponding to $T_n = 0.98 - 1.29$ GeV.

By taking the measured spectator four-momentum into account and reconstructing that way the effective \sqrt{s} for each event, we obtain angular distributions for six \sqrt{s} bins as shown in Fig. 2. Our data agree well with previous experimental results from Saturne for backward [17] angles in the overlap region. Where overlapping our results are also in reasonable agreement with the old Birmingham data [22], which were discarded in previous SAID analyses, though they were taken over nearly the full angular range at $T_p = 0.991$ GeV. Our data are also in

good agreement with the old Berkeley data taken at $T_p = 1.243$ GeV over the full forward angular range [23].

COMPARISON TO EXISTING PARTIAL-WAVE SOLUTIONS

In Fig. 2 the data are compared to recently obtained GWU/SAID partial-wave solutions. The dotted lines resemble the solution SP07 [25], which is based on NN scattering data available until 2007. The dashed curves represent the solution SM16 [26], which in addition is based on forward-angle pp -scattering data from COSY-ANKE. Both these solutions do not include the pole of $d^*(2380)$ and hence do not provide a good description for the np analyzing power data [1, 2] measured by WASA-at-COSY in the region of the $d^*(2380)$ resonance as depicted in Fig. 3. These analyzing power data, however, were included in the solution AD14 resulting in a resonance pole for $d^*(2380)$ in the coupled ${}^3D_3 - {}^3G_3$ partial waves [1, 2, 27]. This solution is denoted by solid lines in Figs. 2 and 3.

Whereas the SP07 and SM16 solutions give very similar results and provide only a qualitative description of the differential cross section data, the AD14 solution succeeds to describe these data already quantitatively — with the exception of the Birmingham data at $T_p = 0.991$ GeV [22] and the backangle data of Bizard et al. at $T_p = 1.252$ GeV [17].

PARTIAL-WAVE ANALYSES INCLUDING THE NEW CROSS SECTION DATA

The WASA-at-COSY cross section data were also included in the GWU/SAID data base for a new partial-wave analysis. Since the AD14 solution gives already a quantitative description for the new cross section data, it is of no surprise that the inclusion of these data in the new partial-wave analysis has no big impact and hence the resulting new solution AD19 is only marginally different from the AD14 solution. The small differences between AD14 and AD19 solutions may serve as a measure of the uncertainties in these solutions.

In order to check the uniqueness of these solutions many fits were carried out with varying initial weights for different data sets and other starting conditions. In this attempt, indeed a solution SM20 was found, which comes closer to the analyzing power data than the previous solutions SP07 and SM16 did — as depicted in Fig. 3. However this solution does much worse than AD14 and AD19 for the differential cross sections — see Figs. 2, where SM20 appears to be very close to the SP07 and SM16 results.

In order to investigate the SM20 solution in some more detail, we compare the various GWU/SAID solutions in

Fig. 4 with the WASA high-statistics data for the angular distribution of the analyzing power in the $d^*(2380)$ region (left panel) as well as with the energy dependence of the analyzing power near 90° (right panel). As pointed out in Refs. [1, 2], the contribution of $d^*(2380)$ in the analyzing power is proportional to the associated Legendre polynomial $P_3^1(\cos\Theta_n^{cm})$. Therefore the resonance effect is at maximum in the 90° region. Due to the richer data base at 85° we prefer to show the energy dependence not for exactly 90° , but for 85° on the right panel in Fig. 4.

The WASA high-statistics data shown in the left panel of Fig. 4 were obtained by not accounting for the spectator momentum. Thus these data represent a weighted average over the measured interval $\sqrt{s} = 2.37 - 2.40$ GeV ($T_n = 1.11 - 1.20$ GeV) with a centroid at $\sqrt{s} = 2.38$ GeV — see Fig. 1 in Ref. [1] and Fig. 4 in Ref. [2], respectively. We see that for the various partial-wave solutions the most critical angular region is around 90° , *i.e.* exactly the region which is most sensitive to the $d^*(2380)$ resonance. Whereas AD14 and AD19 solutions reproduce the experimental data very well in this region, the other solutions miss the data there. Most striking is the failure of SP07. SM16 does a bit better and SM20 comes still closer, but nevertheless fails quantitatively in this angular region.

In the right panel of Fig. 4 we explore the energy dependence of the analyzing power in this angular region. There the data exhibit a pronounced pattern resembling the interference of a narrow resonance with the background. The solutions AD14 and AD19 are able to reproduce this pattern quantitatively, though the data suggest a somewhat narrower resonance pattern at the high-energy side¹. The SP07 solution predicts a smoothly curved energy dependence, which is far off the data, whereas the SM16 and SM20 solutions exhibit a somewhat flatter energy dependence coming thus closer to the data on average, but still severely miss the resonance structure in the energy region of $d^*(2380)$.

We conclude that the solutions SP07, SM16 and SM20 all fail in a quantitative description of both cross section and analyzing power data in the energy region of $d^*(2380)$, whereas the solutions AD14 and AD19 can account quantitatively for all experimental data.

In Fig. 5 we plot the 3D_3 and 3G_3 partial-wave amplitudes as well as their mixing term ϵ_3 in dependence of the center-of-mass energy $W = \sqrt{s}$ for the solutions AD14 (solid), AD19 (dash-dotted) and SM20 (dashed). The amplitudes for the AD14 and AD19 solutions are very close and differ slightly only at high energies. Both solutions exhibit a clear resonance structure in the $d^*(2380)$ region in both real and imaginary parts of all three am-

¹ This would be in accord with a slightly narrower resonance width as it is observed in fact in the $NN \rightarrow NN\pi\pi$ channels [4].

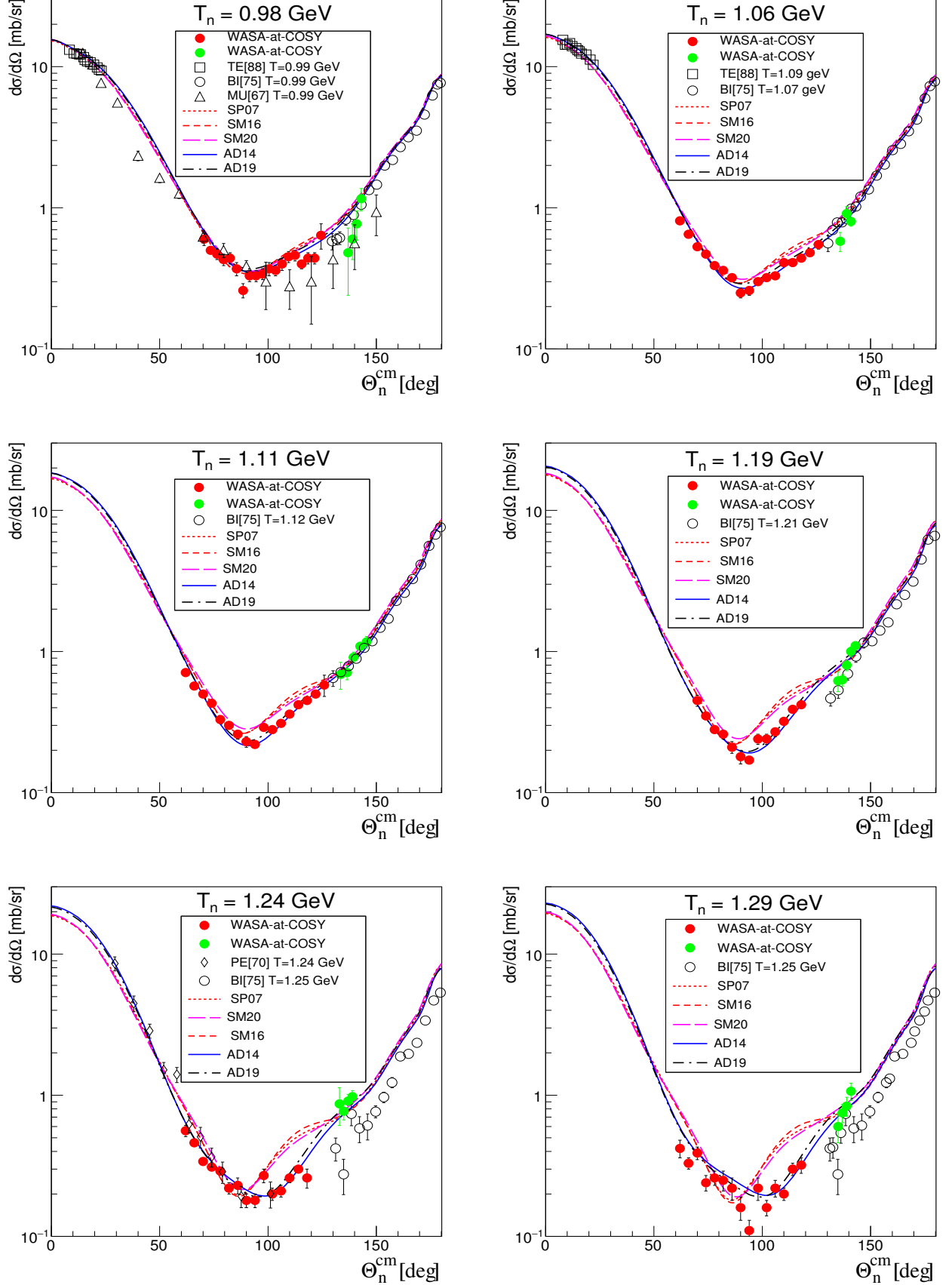


FIG. 2: (Color online) Differential cross sections for elastic np scattering at $T_n = 0.98, 1.06, 1.11, 1.19, 1.24$ and 1.29 GeV corresponding to $\sqrt{s} = 2.32, 2.35, 2.37, 2.40, 2.42$ and 2.44 GeV. The full symbols denote results from this work taking into account the spectator four-momentum information. Open symbols refer to previous measurements: for "TE[88]" see Ref.[16], for "BI[75]" see Ref.[17], for "MU[67]" see Ref.[22] and for "PE[70]" see Ref.[23]. The drawn curves represent various GWU/SAID solutions discussed in the text.

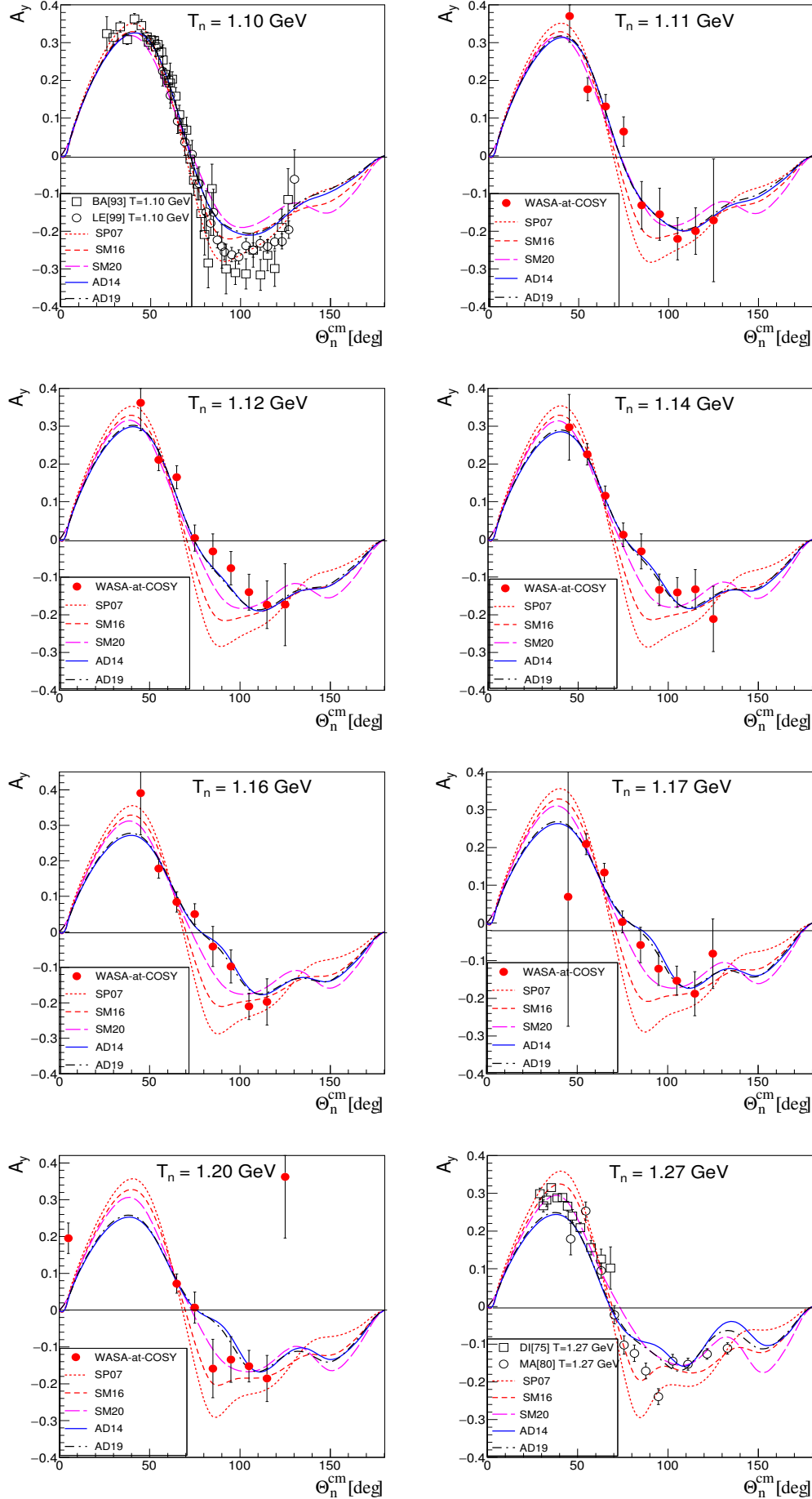


FIG. 3: Same as Fig. 2, but for angular distributions of the analyzing power. The full symbols denote results from WASA-at-COSY [1, 2]. Open symbols refer to previous measurements: for "BA[93]" see Ref.[31], for "LE[99]" see Ref.[32], for "DI[75]" see Ref.[22] and for "MA[80]" see Ref.[24].

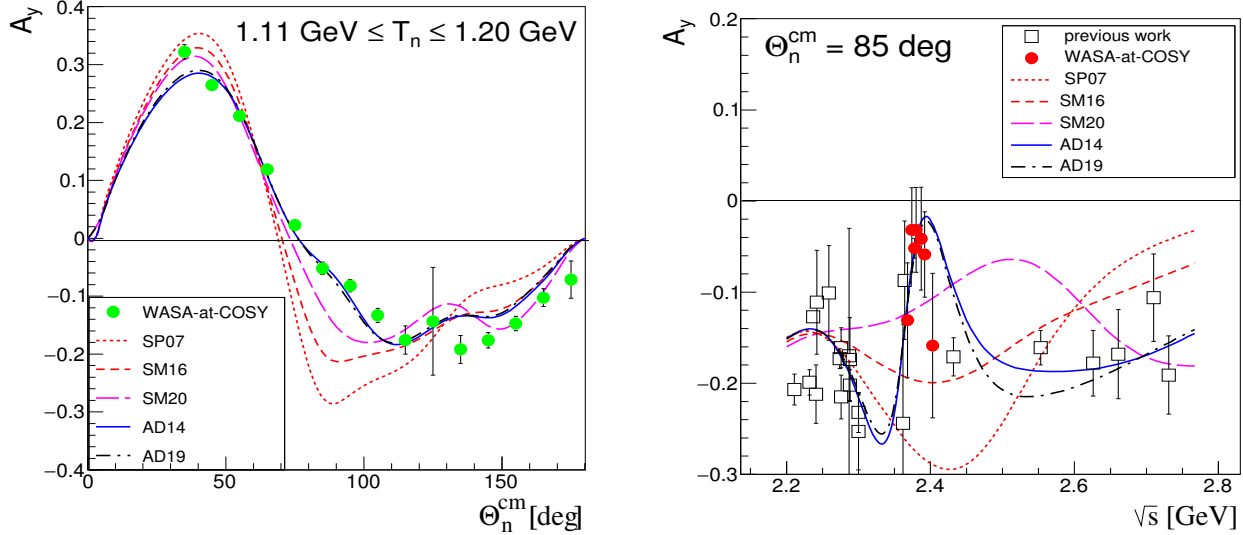


FIG. 4: Same as Fig. 3, but for the angular distribution of the analyzing power averaged over the resonance region ($1.11 \text{ GeV} \leq T_n \leq 1.20 \text{ GeV}$) (left) and the energy dependence of the analyzing power at $\Theta_n^{cm} = 85^\circ$ (right). Filled circles denote the WASA results [1, 2], the open squares show previous experiments [31–39].

plitudes. In contrast, the SM20 solution exhibits only a very smooth energy dependence without indication of any resonance.

In Fig. 6 we plot the Argand diagrams for the 3D_3 (top) and 3G_3 (middle) partial waves and their mixing amplitude ϵ_3 (bottom) for the GWU/SAID solutions SM20 (magenta, dashed), AD14 (blue, solid) and AD19 (black, dash-dotted). Whereas the SM20 solution shows no obvious looping in these diagrams, *i.e.* no sign of a pole, the solutions AD14 and AD19, which nearly coincide, do exhibit pronounced loops in accordance with the presence of the $d^*(2380)$ pole.

PARTIAL-WAVE ANALYSIS AND DATA INTERPRETATION

In the following the search for poles presented in ref. [2], based on analyzing Argand diagrams and the speed plot, is improved. Namely, a looping in the Argand diagram is in the mathematical sense only a necessary condition for the existence of a pole, but not yet a sufficient one. This simply means that, if a function has a pole, it must produce a backward looping, however a backward looping found in Argand diagrams can be produced also by other effects. It E.g., a backward looping in the Argand diagram can be produced by branch-points caused by channel openings — in our case by the nearby $NN^*(1440)$ threshold. To prove definitely that we indeed have a pole we need a more stringent method. Therefore, instead of analyzing Argand diagrams of 3D_3 , 3G_3 , and mixing term ϵ_3 we

introduce the trace of the $^3D_3 - ^3G_3$ matrix, and instead of quantifying the 3D_3 partial wave with the speed plot technique we quantify the whole trace with the Laurent+Pietarinen(L+P) expansion.

The coupled partial waves in question are creating the following $I(J^P) = 0(3^+)$ mixing matrix.

$$T = \begin{bmatrix} ^3D_3 & \epsilon_3 \\ \epsilon_3 & ^3G_3 \end{bmatrix} \quad (2)$$

Without the loss of generality this matrix can be given by its Laurent decomposition in its area of convergence:

$$T = \begin{bmatrix} \frac{a_{11}+ib_{11}}{Den} + B_{11} & \frac{a_{12}+ib_{12}}{Den} + B_{12} \\ \frac{a_{12}+ib_{12}}{Den} + B_{12} & \frac{a_{22}+ib_{22}}{Den} + B_{22} \end{bmatrix} \quad (3)$$

$$Den = M - W - i\Gamma$$

The 3D_3 , 3G_3 partial waves and the mixing term ϵ_3 are given in Fig. 5 for the GWU/SAID solutions SM20 (magenta, dashed), AD14 (blue, solid) and AD19 (black, dash-dotted).

Following the idea presented in ref. [28] we use the

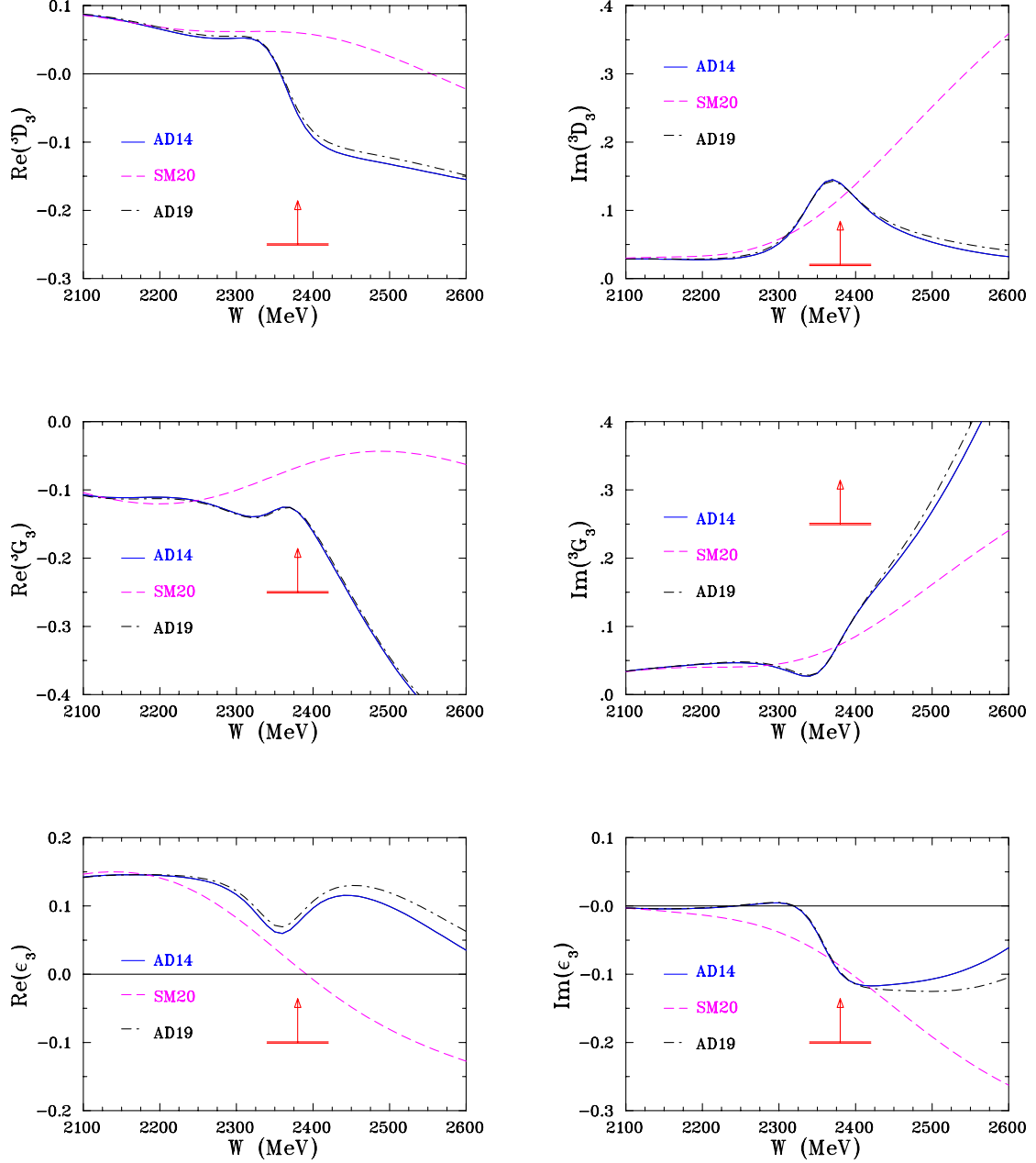


FIG. 5: Real (left) and imaginary (right) parts of the 3D_3 (top), 3G_3 (middle) partial wave amplitudes and the mixing term ϵ_3 (bottom) for the GWU/SAID solutions SM20 (magenta, dashed), AD14 (blue, solid) and AD19 (black, dash-dotted). Vertical arrows with horizontal bar indicate the location of mass and width of $d^*(2380)$.

trace² of $I(J^P) = 0(3^+)$ mixing matrix:

$$\text{Trace}[\mathbf{T}] = \frac{(a_{11} + a_{22}) + i(b_{11} + b_{22})}{\text{Den}} + (B_{11} + B_{22}).$$

² Trace of the matrix is defined as the sum of diagonal matrix elements, and due to its commutativity as $\text{Trace}(\mathbf{A} \cdot \mathbf{B}) = \text{Trace}(\mathbf{B} \cdot \mathbf{A})$ it is identical for all matrices obtained from the original matrix by $U^{-1} \cdot \mathbf{A} \cdot U$; hence for the diagonal one too.

As it has been shown in that reference, structures which are buried under notable background in individual matrix elements pop out once the trace of the matrix is done. In Fig. 7 we show the trace of all three GWU/SAID solutions.

The quantitative evaluation of the pole parameters of the Trace [T] is done using the Laurent+Pietarinen (L+P) formalism identical to the way how it has been

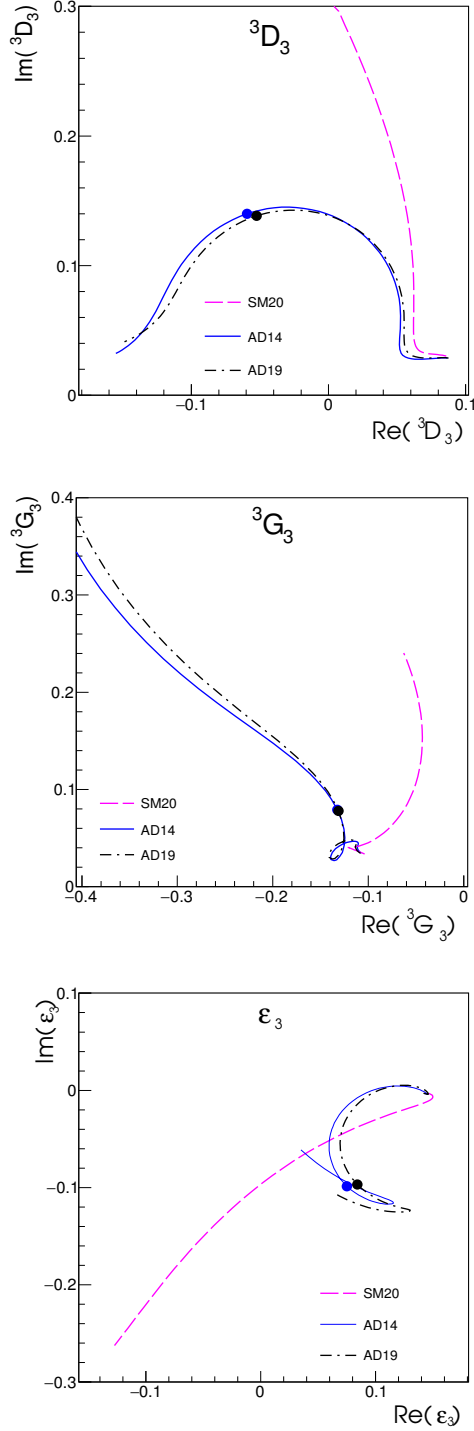


FIG. 6: Argand diagrams for the 3D_3 (top) and 3G_3 (middle) partial wave amplitudes and their mixing term ϵ_3 (bottom) for the GWU/SAID solutions SM20 (magenta, dashed), AD14 (blue, solid) and AD19 (black, dash-dotted). The thick dots display the $d^*(2380)$ pole position

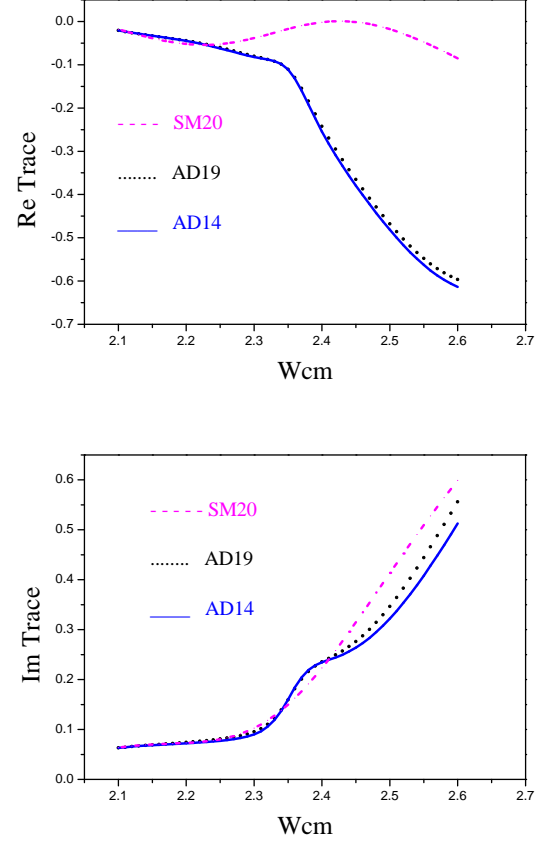


FIG. 7: The Trace of all three GWU/SAID partial-wave solutions SM20 (magenta, dashed), AD14 (blue, solid) and AD19 (black, dotted) solutions.

done in ref. [29]. For the convenience of the reader let us repeat some basic facts.

The driving concept behind the method is to replace the complexity of solving an elaborate theoretical model and analytically continuing its solution into the complex energy plane by using a local power-series representation of partial wave amplitudes which just exploits analyticity and unitarity. The L+P approach separates pole and regular part in the form of a Laurent expansion, and instead of modeling the regular part using some physical model it uses the conformal-mapping-generated, rapidly converging power series with well defined analytic properties called a Pietarinen expansion to represent it effectively. In other words, the method replaces the regular part calculated in a model with the simplest analytic function which has correct analytic properties of the analyzed partial wave (multipole), and fits the given input. In such an approach the model dependence is minimized, and is reduced to the choice of the number and location of L+P branch-points used in the model.

So, we expand the trace in terms of a sum over all poles and with a Pietarinen series representing the energy

dependent regular (non-pole) part as:

$$\text{Trace}[T] = \sum_{i=1}^k \frac{\alpha_{-1}^{(i)}}{W - W_i} + B^L(W). \quad (5)$$

Here W , $\alpha_{-1}^{(i)}$, and W_i are complex numbers representing the c.m. energy, residues, and pole positions for the i th pole, respectively, and $B^L(W)$ is a regular function in the whole complex plane. As it has been shown in Ref. [30] the generally unknown analytic function $B(W)$ with branch-points in x_P , x_Q , and x_R can be expanded into a power series of Pietarinen functions as

$$\begin{aligned} B^L(W) &= \sum_{n=0}^M c_n X(W)^n + \sum_{n=0}^N d_n Y(W)^n \\ &+ \sum_{n=0}^N e_n Z(W)^n + \dots, \\ X(W) &= \frac{\alpha - \sqrt{x_P - W}}{\alpha + \sqrt{x_P - W}}, \\ Y(W) &= \frac{\beta - \sqrt{x_Q - W}}{\beta + \sqrt{x_Q - W}}, \\ Z(W) &= \frac{\gamma - \sqrt{x_R - W}}{\gamma + \sqrt{x_R - W}} \end{aligned} \quad (6)$$

where c_n , d_n , e_n and α , β , γ are real numbers that represent tuning parameters and coefficients of the Pietarinen functions $X(W)$, $Y(W)$, and $Z(W)$, respectively. A variable number of coefficients in the three series of Eq. (6) was used, depending on the structure of the non-pole part of each amplitude.

As the nearby energy points of the input partial-wave trace are correlated through analyticity of the energy dependent partial wave of the GWU/SAID solutions, the standard error analysis cannot be used as the standardly defined χ^2 becomes extremely small ($\chi^2 \ll 1$) regardless which error is attributed to the input. The method used is identical to what has been done in ref. [29], and is based on randomizing the central values of the energy dependent (ED) solution with partial-wave (PW) standard deviation σ_{PW} , and assigning the error of the source ED point as the error of the randomized point. In that way we generate 1000 different sets which are analyzed by L+P, and the error analysis is done in a standard way for non-correlated quantities.

At this point it is important to stress that our central problem is to establish whether the analyzed GWU/SAID solutions contain a pole or not. The L+P approach by construction detects resonances in two different ways: either as a resonance in a two-body process, which manifests itself as a pole on the real axes, or a resonance in the three body sub-system, which manifests itself as a complex branch-point. In either of the two cases we encounter a resonance; however, there is still

the matter of identifying its location with the purpose of its identification.

The difference between the two situations is subtle. If we have a genuine pole in the two-body system, our real and imaginary parts will show a typical resonance behaviour, and real branch-points which represent the opening of two-body channels consisting of two stable particles should be in principle clearly visible as they produce sharp cusps in the analyzed amplitude. However, where the branch-point represents a channel which consists of a stable particle and a two-body resonant state, this branch-point will become complex, and the sharp, cusp effect disappears. These two processes are different, but the method will require much higher precision of the data to distinguish between the two. Just by looking at figure Fig. 7 it is clear that our process will strongly depend on the confidence limit of all obtained GWU/SAID solutions. Namely, in the ideal case, when the confidence limit is high and the error band is low, the method will be able to distinguish between the two. However, as soon as error bands become realistic, the clearly visible peak in the imaginary part will be smeared out, and the distinction between the two scenarios (genuine pole or complex branch-point) will be lost.

Therefore, we produce three sets of results: solution a) given in Table I with estimated error of 0.1 %; solution b) with error increased by five times to 0.5 %; and c) in Table II with realistic error of the GWU/SAID solutions estimated to be 2 %.

What we immediately see from the tables is that the clearness of the effect is the bigger the smaller the error bars are, and that is what we expected. A pole is certainly detected for AD14 and AD19 solutions, but it is not clear, whether it is a real two-body resonance in two-body system materialized as a genuine pole, or a two-body resonance in the three-body subsystem materialized as a complex branch-point. For the third SM20 solution the possibility of the pole in a form of complex branch-point is preferred only for ideal cases with unrealistically small error bars, but for realistic error bars the situation is ambiguous. For the smallest error bars in Table I we see that all three solutions including SM20 require at least a complex branch-point, but for the realistic error in Table II it is only clear that real branch-points are much less likely for all three solutions (χ_{df}^2 is the biggest, but not convincingly). On the other hand, for the ideal case given in Table I it is very likely that these results could be interpreted only as a resonance in the two-body system as χ_{df}^2 is notably higher for the other two possibilities - real and complex branch-points. Our test with errors of 0.5 % shows that already in this case equal probability for real pole and complex branch-point solution is reached.

Therefore, we may conclude:

Both AD solutions require a pole in the system, how-

TABLE I: List of results for resonance poles and branch points (bp) for the ideal case with errors of 0.1 %. Values in brackets denote estimated uncertainties.

| | | SM20 | AD19 | AD14 |
|--------------------------------------|------------------|---------------------|----------------------|----------------------|
| χ^2_{df} | real bp | 59.5(2) | 263.7(41.4) | 435(314) |
| | cmplx bp | 1.1(0.7) | 10.97(0.6) | 8.8(0.7) |
| | real bp + 1-pole | | 2.34(0.3) | 2.0(0.4) |
| resonance in 3-body sub-system | real b.p. | | | |
| | cmplx bp | 2260(22) - i 64(44) | 2352(1) - i 54(2) | 2348(1) - i 48(2) |
| | real + bp 1-pole | | | |
| genuine 2-body resonance | real bp | | | |
| | cmplx bp | | | |
| | real bp + 1-pole | | 2362(0.7) - i 114(2) | 2362(0.6) - i 109(2) |

TABLE II: Same as Table I, but for a realistic error of 2 %.

| | | SM20 | AD19 | AD14 |
|--------------------------------------|------------------|--------------------|----------------------|---------------------|
| χ^2_{df} | real bp | 1.38(0.3) | 1.83(0.2) | 2.06(0.3) |
| | cmplx bp | 0.97(0.16) | 0.99(0.16) | 0.98(0.16) |
| | 1-pole | | 1.03(0.15) | 1.08(0.5) |
| resonance in 3-body sub-system | real bp | | | |
| | cmplx bp | 2265(76) - i 0 (7) | 2361(14) - i 59 (21) | 2354(12) - i 44(20) |
| | real bp + 1-pole | | | |
| genuine 2-body resonance | real bp | | | |
| | cmplx bp | | | |
| | real bp + 1-pole | | 2361 (21) - i 63(20) | 2361(11) - i 60(13) |

ever the distinction between a pole in the two-body system or one in the three-body subsystem depends on the reliability of the GWU/SAID solutions. The numerical quantification also depends on the confidence limit of the GWU/SAID solutions.

However, if we add information from sources other than just elastic pn scattering, then the complex branch-point solution can be safely discarded. As noted already above, the only possible 3-body branch point in the vicinity of the found pole location is due to the $NN^*(1440)$ configuration. The Roper resonance $N^*(1440)$ is much broader than suggested by the imaginary part of the pole given in Table II. And since it is formed near threshold in the isoscalar part of the $NN \rightarrow NN^*(1440)$ reaction preferentially by the 3S_1 NN partial wave, a significant formation by the isoscalar $^3D_3 - ^3G_3$ partial waves appears very unlikely. Finally, $d^*(2380)$, which may be identified with the found pole, does not decay into $NN^*(1440)$ (BR < 14% at 90% C.L.) according to the recent measurement of the isoscalar part of the $NN \rightarrow NN\pi$ reaction [10].

In our tests with various different error assignments to the GWU/SAID solutions the location of the pole position appears to be remarkable stable against these 1error variations. The result of 2361(16) MeV is compatible with the traditional speed plot result of 2380(10) MeV

[2] within uncertainties as well as with the result from the $np \rightarrow d\pi^0\pi^0$ reaction [4], where a value of 2.37 GeV was observed for the $d^*(2380)$ resonance energy.

The situation with respect to the resonance width is more delicate. Though the width deduced with the L+P method still overlaps within uncertainties with that deduced by the speed plot technique of 80(10) MeV, it is at notable variance with the result of 70 MeV from $np \rightarrow d\pi^0\pi^0$. There are several reasons for this discrepancy. First, as already noted in the discussion of the energy excitation function of the analyzing power around 90° — where the resonance effect of $d^*(2380)$ is largest — the measured resonance structure at the high-energy side is narrower than accounted for by the AD solutions. This failure causes a long high-energy tail of the resonance structure seen in $Im(^3D_3)$, Fig. 5 top right. In consequence, the resonance effect appears to more extended in the PW solutions than in the data. Secondly, high-quality data beyond $\sqrt{s} = 2.44$ GeV are rare in the GWU/SAID data base and hence the uncertainties in the various PW solutions increase rapidly beyond this energy. *I.e.* the high-energy tail of the $d^*(2380)$ resonance is not well fixed in the PW solutions causing a large uncertainty in the separation of pole and background. This is particularly true for the L+P method, where the resonance shape is kept unconstrained as much as possible. Hence

the true uncertainties for the imaginary part of the pole appear to be even larger than given in Table II.

SUMMARY AND CONCLUSIONS

New data for the differential cross sections in the energy region of the $d^*(12380)$ dibaryon resonance have been presented. They were extracted from exclusive and kinematically complete measurements of quasifree $\bar{n}p$ scattering using the WASA detector setup at COSY and having a polarized deuteron beam impinged on the hydrogen pellet target. The new cross section data supplement the analyzing power data published already earlier [1, 2].

The new cross section data are at obvious variance with the GW/SAID partial-wave solutions SP07, SM16 and SM20, however, agree quantitatively with the solutions AD14 and AD19. Whereas the first ones do not contain the $d^*(2380)$ pole, the latter two do include this pole. The solution AD14 was obtained 2014 by inclusion of the WASA analyzing power data into the SAID data base. These data then produced the $d^*(2380)$ pole in the coupled $^3D_3 - ^3G_3$ coupled partial wave. It is very gratifying and simultaneously demonstrates the predictive power of this solution that it is able to provide a quantitative description of the new data on the differential cross sections. The new solution AD19, which includes now also the new cross section data in the SAID data base, deviates from the AD14 solution only marginally.

Since a looping in the Argand diagram is a necessary condition for a resonance pole, but not yet a sufficient one, the three GWU/SAID solution AD14, AD19 and SM20 were subjected to an interpretation within the Laurent+Pietarinen method. The conclusion there is that a pole at the position of the $d^*(2380)$ resonance is clearly confirmed. However understanding the effect as a consequence of the $NN^*(1440)$ branch-point in the 3-body sub-channel can be excluded definitely only by using additional information about the isoscalar part of the $NN \rightarrow NN\pi$ reaction. Based on the elastic pn scattering alone, a strict elimination of the branch-point interpretation would necessitate new precise high-quality measurements, in particular at energies beyond $\sqrt{s} = 2.4$ GeV, in order to approach the precision given in Table I.

ACKNOWLEDGMENTS

We acknowledge valuable discussions with C. Hanhart and C. Wilkin on this issue. This work has been supported by BMBF, Forschungszentrum Jülich (COSY-FFE) and the German Research Foundation DFG (CL214/3-2 and 3-3). Three of us (H. Cl., I. S. and A. Š) appreciate the support by the Munich Institute for Astro- and Particle Physics (MIAPP) which is

funded by the Deutsche Forschungsgemeinschaft (DFG, German Research Foundation) under Germany's Excellence Strategy – EXC-2094 - 390783311. This work was supported (W.B., I.S. and R.W.) in part by the U. S. Department of Energy, Office of Science, Office of Nuclear Physics under Awards No. DE-SC0016583 and DE-SC0016582.

* present address: Albert Einstein Center for Fundamental Physics, University of Bern, Sidlerstrasse 5, 3012 Bern, Switzerland

† present address: Department of Physics and Astrophysics, University of Delhi, Delhi-110007, India

‡ present address: Dipartimento di Fisica dell'Università Sapienza, Roma, Italy and INFN Sezione di Roma, Roma, Italy

§ present address: Institut für Kernphysik, Johannes Gutenberg-Universität Mainz, Johann-Joachim-Becher Weg 45, 55128 Mainz, Germany

¶ present address: Department of Physics and Astronomy, University of Sheffield, Hounsfield Road, Sheffield, S3 7RH, United Kingdom

- [1] P. Adlarson *et al.*, Phys. Rev. Lett. **112**, 202301 (2014).
- [2] P. Adlarson *et al.*, Phys. Rev. C **90**, 035204 (2014).
- [3] M. Bashkanov *et al.*, Phys. Rev. Lett. **102**, 052301 (2009).
- [4] P. Adlarson *et al.*, Phys. Rev. Lett. **106**, 242302 (2011).
- [5] P. Adlarson *et al.*, Phys. Lett. B **721**, 229 (2013).
- [6] P. Adlarson *et al.*, Phys. Rev. C **88**, 055208 (2013).
- [7] P. Adlarson *et al.*, Phys. Lett. B **743**, 325 (2015).
- [8] G. Agakishiev *et al.*, Phys. Lett. B **750**, 184 (2015).
- [9] H. Clement, M. Bashkanov and T. Skorodko, Phys. Scr. T166, 014016 (2015).
- [10] P. Adlarson *et al.*, Phys. Lett. B **774**, 599 (2017).
- [11] M. Bashkanov, H. Clement and T. Skorodko, Eur. Phys. J. A **51**, 87 (2015).
- [12] H. Clement, Prog. Part. Nucl. Phys. **93**, 195 (2017).
- [13] A. Gal, Phys. Lett. B **769**, 436 (2017).
- [14] T. Ishikawa *et al.*, Phys. Lett. B **772**, 398 (2017).
- [15] Proc. HADRON 2017, PoS **310**, 051 (2017).
- [16] Y. Terrien *et al.*, Phys. Rev. Lett. **59**, 1534 (1987).
- [17] G. Bizard *et al.*, Nucl. Phys. B **85**, 14 (1975).
- [18] J. Bystricky *et al.*, J. Phys. **48**, 1901 (1987).
- [19] Chr. Bargholtz *et al.*, Nucl. Inst. Meth. A **594**, 339 (2008).
- [20] H. H. Adam *et al.*, arxiv: nucl-ex/0411038.
- [21] R. Machleidt, Phys. Rev. C **63**, 024001 (2001).
- [22] T.A. Murray *et al.*, Nuov. Cim. **49**, 261 (1969).
- [23] M.L. Perl *et al.*, Phys. Rev. D **1**, 1857 (1970).
- [24] SAID data base <http://gwdac.phys.gwu.edu/>;
- [25] R. A. Arndt *et al.*, Phys. Rev. C **76**, 025209 (2007).
- [26] R. Workman, W. Briscoe and I. Strakovsky, Phys. Rev. C **94**, 065203 (2016).
- [27] R. Workman, W. Briscoe and I. Strakovsky, Phys. Rev. C **93**, 045201 (2016).
- [28] S. Ceci, A. Švarc, B. Zauner, D.M. Manley, S. Capstick, Phys. Lett. B **659** 228-233 (2008).
- [29] W.J. Briscoe *et al.*, Phys. Rev. C **100**, 065205 (2019).
- [30] A. Švarc, M. Hadžimehmedović, H. Osmanović, J. Sta-

- hov,, L. Tiator, and R. L. Workman, Phys. Rev. C **88**, 035206 (2013).
- [31] J. Ball *et al.*, Nucl. Phys. A **559**, 489 (1993).
 - [32] A. de Lesquen *et al.*, Eur. Phys. J. C **11**, 69 (1999).
 - [33] R. Diebold *et al.*, Phys. Rev. Lett. **35**, 632 (1975).
 - [34] Y. Makdisi *et al.*, Phys. Rev. Lett. **45**, 1529 (1980).
 - [35] C. R. Newsom *et al.*, Phys. Rev. C **39**, 965 (1989).
 - [36] J. Arnold *et al.*, Eur. Phys. J. C **17**, 67 (2000).
 - [37] J. Ball *et al.*, Nucl. Phys. B **286**, 635 (1987).
 - [38] M. W. McNaughton *et al.*, Phys. Rev. C **48**, 256 (1993); **53**, 1092 (1996).
 - [39] G. Glass *et al.*, Phys. Rev. C **47**, 1369 (1993).